Electrical Power and Energy Systems 118 (2020) 105834

Contents lists available at ScienceDirect

Electrical Power and Energy Systems

journal homepage: www.elsevier.com/locate/ijepes

Forecast-based overcurrent relay coordination in wind farms

Sujo P. George*, S. Ashok

Electrical Engineering Department, National Institute of Technology Calicut, Kerala, India

ARTICLE INFO

Keywords:
Over current relays
Relay coordination
Wind direction
Wind farms
Wind generators
Wind speed
Wind speed forecasting

ABSTRACT

Relay coordination ensures the appropriate isolation of healthy feeders from the faulty areas in a power system. The dynamic nature of renewable sources such as wind generators (WGs) can create variations in fault levels which affect the relay settings. This causes coordination problems, which can lead to the faulty operation of overcurrent relays (OCRs). The settings of the relay need to be modified appropriately in line with the variations of fault levels, which in turn change with the wind dynamics. As a solution, wind forecast based technique for the coordination of the OCRs in wind-integrated substations is suggested in this work. In the proposed algorithm, wind speed and its direction are predicted and the settings of the relay are predetermined using an optimization technique. This reduces the computation time required for the algorithms in the current period. The algorithm is implemented in the modified IEEE 9-bus system with wind farms and also in a typical wind-integrated substation. Further, it is validated through an experimental setup in the laboratory. The results were found to be promising and the algorithm can be applied to any substations integrated with wind farms for avoiding relay mal-operations.

1. Introduction

Wind power generation is emerging as the fastest developing technology providing the largest share of the distributed generations. The total installed capacity of power generation from the wind has been increasing annually at an average of about 20% across the world [1,2]. The integration of wind farms with power networks is intermittent, according to the operating conditions of the WGs [3,4]. Wind farms are usually connected to the distribution feeders and then integrated into the grid. The most commonly used protection scheme for the feeders is the inverse type of overcurrent protection. The OCRs in the distribution feeders should be coordinated with their backup relays in the main feeders which connects the distribution feeders to the grid [5,6]. The settings of the OCRs are fixed at the rated capacities of the connected load and the wind farm. The penetration of wind farms into the power grid changes the conventional distribution system's short-circuit power causing malfunctions and coordination problems in OCRs, as reported in [7]. Therefore, the settings of the relays need to be modified according to the various operating condition of the WGs.

The methods commonly adopted to determine the relay settings are the conventional approaches and optimization techniques [8]. The conventional method is to predetermine all fault currents during abnormal conditions and system contingencies. Conventional methods are based on network topology which includes graphical selection procedure, identification of the minimum break point set and linear graph theory [9–11]. In large systems, during contingencies the conventional method is not applicable since it is time-consuming to update with the new relay settings [8]. In a power network the relay coordination with multiple distributed generators becomes unfeasible via conventional techniques [12]. Therefore, optimization methods are proposed to minimize the total operating time of the relays subjected to the constraints. In linear programming (LP), the plug settings (PS) are predetermined and the operating time of the relays is calculated by optimizing the time multiplier settings (TMS) [13,14]. These methods are not capable of handling complicated problems, especially in large interconnected ring systems and the obtained results may be trapped in local minimum values [15]. Therefore, the coordination problem is formulated as a nonlinear programming technique where the PS and TMS are determined simultaneously [16]. Many heuristic optimization techniques like genetic algorithms (GAs) [17], particle swarm optimization techniques [18], differential evolution algorithms (DEs) [19] and ant colony optimization [20], have been proposed which gives better results but are time-consuming. Therefore, the relay coordination problem is solved by adding suitable penalty functions in large interconnected networks [21]. A hybrid method combining cuckoo search (CS) and GA with linear programming is proposed in [22] and [23] respectively. The hybrid algorithm has better accuracy, computational efficiency and provides lower operating time for the relays by

* Corresponding author.
E-mail address: sujop709@gmail.com (S.P. George).

https://doi.org/10.1016/j.ijepes.2020.105834
Received 14 September 2019; Received in revised form 2 December 2019; Accepted 5 January 2020

maintaining the coordination time interval (CTI).

The wind power and the current from wind farms are dynamic in nature, which in turn can affect the relay settings. From the discussions, it is clear that the relay settings need to be adaptive in line with the wind speed and wind direction. The delay in determining the relay settings from the tail end and its coordination with other relays can cause malfunctioning of the OCRs. A considerable amount of delay time can be avoided if the relay settings in line with the predicted wind speed and wind direction are calculated in advance. An algorithm which can forecast the wind speed and its direction and optimize the relay settings according to the predicted wind-farm current is proposed in this work. The methods of artificial intelligence for predicting the wind parameters are hybrid adaptive neuro-fuzzy inference system (ANFIS) and seasonal auto regression integrated moving average (SARIMA), whereas hybrid DE-LP approach was used for optimal relay coordination. The proposed algorithm is implemented in the modified IEEE 9-bus system with wind farms and also in a typical wind-integrated substation, which were used for validating the developed model. The final stage involves verification of the algorithm using the radial feeder protection unit in the laboratory.

2. Problem formulation

The contribution of fault current from the WGs in wind farm is variable in nature, according to the variation in wind speed and wind direction. Hence the relay settings need to be modified in line with the variation of the fault level, which in turn changes with the wind-power penetration. This can be achieved in two steps which include the wind forecasting and predetermination of optimal relay settings. The wind speed and direction is predicted for the particular wind-farm location and the fault current is calculated. In an interconnected ring system, the complexity of the relay coordination problem requires an optimization framework to obtain the accurate relay settings. Therefore, the optimal TMS and PS values are compared using the different optimization techniques, and the better method is coupled with the proposed forecasting algorithm.

2.1. Hybrid ANFIS-SARIMA forecasting method

A hybrid methodology combining empirical mode decomposition (EMD), ANFIS and SARIMA techniques [24,25] are implemented for the proposed forecasting method. Let ΔT be the time interval for the prediction, ΔT_p the time taken by the algorithm to calculate the wind power output and ΔT_o the time taken by the optimization algorithm to calculate TMS and PS. The time required for transferring the setting to the relay is ΔT_r. The total time taken is ΔT_t, i.e., $\Delta T_t = \Delta T_p + \Delta T_o + \Delta T_r$, which must be less than ΔT. Apart from the previous *n-2* intervals, the data (wind speed, wind direction and meteorological conditions) measured in the time from ΔT_t to ΔT in the *n-1* interval is also used in the prediction of n^{th} interval (for better accuracy). The meteorological conditions taken for the proposed forecasting method are temperature, pressure and humidity. In the developed algorithm along with the wind speed and its direction, the temperature, pressure and humidity are also taken into account. The block diagram representation for the proposed wind prediction methodology is shown in Fig. 1. The original data to be forecasted from the wind farm are separated into periodic and non-periodic series using the EMD method. EMD is an effective method for separating the characteristic information from the original data series, and can be disintegrated into a set of intrinsic mode functions (IMFs). The non-periodic data series is forecasted using the ANFIS method, and the SARIMA model is used for predicting the periodic data. The steps involved in the prediction of the wind speed are given in the following steps.

The wind speed data can be separated into IMFs and one residual series is represented as

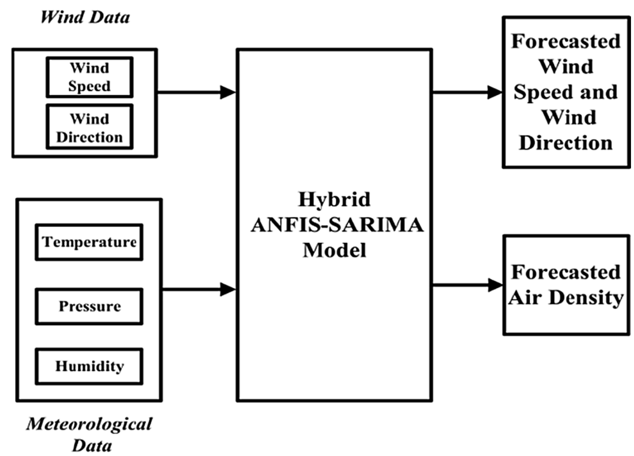

Fig. 1. Hybrid ANFIS-SARIMA model for prediction.

$$V(t) = \sum_{i=1}^{q} I_i(t) + J_k(t) \tag{1}$$

where $I_i(t)$ and $J_k(t)$ are the IMFs and the residual series of the original wind speed series $V(t)$. $H_j(t)$ is used to represent the periodic nature of the series $I_i(t)$ and $J_k(t)$ and otherwise they are defined as $G_i(t)$. Thus, the original wind speed series can be represented as follows:

$$V(t) = \sum_{i=1}^{p} G_i(t) + \sum_{j=p+1}^{q} H_j(t) + J_k(t) \tag{2}$$

where $G_i(t)$ and $H_j(t)$ represent the non-periodic and periodic components of the wind speed series respectively. For $G(t)$ and $J_k(t)$, the ANFIS model is applied to forecast the series and the results are defined as $\bar{G}_i(t)$ and $\bar{J}_k(t)$. The SARIMA model is used to forecast the series $H_j(t)$, and the forecasting result is defined as $\bar{H}_j(t)$.

$$\bar{V}(t) = \sum_{i=1}^{p} \bar{G}_i(t) + \sum_{j=p+1}^{q} \bar{H}_j(t) + \bar{J}_k(t) \tag{3}$$

where $\bar{V}(t)$ is the predicted wind speed. The angle of attack ($\bar{\theta}(t)$) and air density ($\bar{\rho}(t)$) are also predicted using the EMD and hybrid ANFIS-SARIMA methods, for the calculation of power output from WGs.

The mechanical and electrical power output and current from the wind farm are calculated from the predicted wind speed and wind direction. The turbine power output can be written as

$$P_w(t) = \frac{1}{2} C_p A \bar{\rho}(t) (\bar{V}(t) \cos(\bar{\theta}(t)))^3 \tag{4}$$

where the density of air, $\rho(t) = P(t)/(R_{specific}\,T(t))$. The maximum power coefficient is C_p, A is the area swept by the rotor, $V(t)$ is the wind speed, $P(t)$ is atmospheric pressure, $T(t)$ is the atmospheric temperature and $R_{specific}$ is the specific gas density which depends upon the humidity of air. If the wind interacts with the turbine at an angle $\theta(t)$, then the possibility of azimuthal angle variations in the airflow can be taken into account by $\cos(\theta(t))$ [26]. Therefore in the proposed wind speed prediction methodology, $\cos(\theta(t))$ is also taken into consideration and power output is calculated.

The power received by the electrical grid, $P_e(t)$ is obtained as

$$P_e(t) = \eta_{gb} \eta_{gn} P_w(t) \tag{5}$$

where η_{gb} and η_{gn} are the efficiencies of the gearbox and generator. The current from a single WG, I_w, can be calculated using the equation

$$I_w(t) = \frac{P_e(t)}{\sqrt{3} \cos\varphi V_L(t)} \tag{6}$$

where $V_L(t)$ and $\cos\varphi$ are the line voltage and power factor of the system respectively.

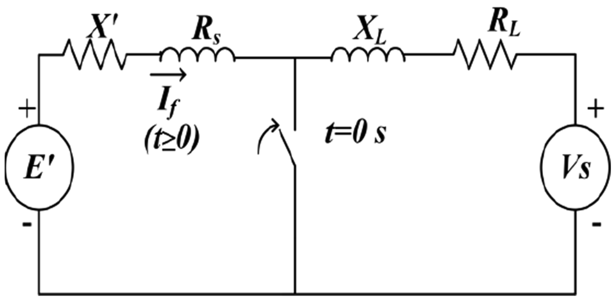

Fig. 2. Sequence network circuit for three phase fault.

2.2. Predetermination of fault current

The contribution of fault current from Type I, Type II and Type V wind generators are about 10–15 times the rated current and remain sustained. The control strategy in the converters and inverters limit the fault current from the Type IV wind generators to 2–3 times the rated current and to an extent in Type III wind generators. However, the fault current contribution from Type III and Type IV WGs is limited to 2–3 cycles. This fault response period is critical for the operation of the protective relays on the interconnected system because, it is during that same time period that the protective relays are determining whether to trip the circuit breakers or not. The RMS value of the fault current, I_f from the squirrel cage induction generator (SCIG) wind machine for a particular instant t, after a three phase short circuit fault occurs is calculated using the network given below (Fig. 2) [27,28].

The initial RMS value of fault current after the switch closes at t = 0 s is given by

$$I_f = \frac{E'}{R_s + jX'} \tag{7}$$

E' and X' are the sub transient internal voltage and sub transient reactance of the generator at the instant of the fault respectively. The sub transient internal voltage of the machine can be expressed as

$$E' = V_s - (R_s + R_L)I_w - j(X' + X_L)I_w \tag{8}$$

where R_s is the stator resistance of the induction machine, V_s is the stator voltage or the source voltage, I_w is the stator current prior to the fault. The resistance and reactance of the line that connects WGs to the grid is given by R_L and X_L. The sub transient reactance X' is calculated using the following equation

$$X' = X_s + \frac{X_m X_2}{X_m + X_2} \tag{9}$$

where X_s is the stator leakage reactance, X_m is the magnetizing reactance, X_2 is the rotor leakage reactance. From the Eqs. (7) and (8), the fault current, I_f for a particular instant can be written as

$$I_f = \frac{V_s - (R_L + jX_L')I_w}{R_s + jX'} - I_w \tag{10}$$

In the Eq. (10), the term I_w can be neglected due to it is lower order compared to term $\frac{V_s - (R_L + jX_L')I_w}{R_s + jX'}$. The values of V_s, R_L, X_L, R_s and X' are constant for a typical SCIG machine. Therefore the fault current from the SCIG depends on I_w which in turn depends on the wind speed (From Eqs. (5), (6) and (10)). The stator current, I_w is at a maximum value when the machine is operating at the rated speed. The stator current, and hence the fault-current contribution, decrease for all other wind speeds. In a wind farm, with n number of WGs, the effect of wind speed and its direction will be different for each generator. Therefore the total power output from the wind farms is varying according to the operating conditions of each WGs. The total fault current from the wind farm, I_{ftot} can be expressed as the summation of the fault currents from the individual WGs. The total fault current from the wind farm and is given in Eq. (11).

$$I_{ftot} = \sum_{g=1}^{n} I_{fg} = \sum_{g=1}^{n} \left(\frac{E'_g}{(R_s + jX')} \right) \tag{11}$$

2.3. Optimal relay coordination

The forecasting algorithm is coupled with the optimization algorithm to discover the settings for the OCRs. The coordination problem in the OCRs is expressed as an optimization problem to minimize the objective function value T, which is the overall operating time of the relays [22,23]. The time of operation t of the OCR is an inverse function of the fault current passing through it. The time-current characteristics of the relay can be expressed as

$$\mathrm{t_{xy}} = \mathrm{TMS_i}\left[\frac{\mathrm{A}}{\left(\frac{\mathrm{I_{sxy}}}{\mathrm{I_{py}}}\right)^{\mathrm{B}} - 1} + \mathrm{C}\right] \tag{12}$$

where y is the relay number, x is the fault location and t_{xy} is the operating time of the y^{th} relay due to a fault in the x^{th} location. A, B and C are scalar quantities and their values depend upon the characteristics of the OCRs. The term I_{sxy} represents the fault current detected by y^{th} relay due to a fault in the x^{th} location and I_{py} represents the pickup current selected for the y^{th} relay.

2.3.1. Objective function

The objective of the optimization problem is to minimize the overall operating time of both main and backup relays, while maintaining the constraints for the relay coordination. The objective function can be expressed as

$$Minimize\ T_o = \sum\nolimits_{x=1}^{U} \left(\sum_{\mathrm{y=1}}^{\mathrm{W}} \mathrm{t_{mxy}} + \sum_{\mathrm{z=1}}^{\mathrm{W}} \mathrm{t_{bxz}} \right) \forall\ (y, z) \in O \tag{13}$$

where O is the set of main and backup pairs of the OCRs, W represents the total number of relays and U is the total number of fault locations in all the feeders of the system. For a fault at location x, the variables t_{mxy},t_{bxz} represents time of operation of the main relay y and backup relay z (Eqs. (14) and (15)).

$$t_{mxy} = TMS_{my}\left[\frac{A}{\left(\frac{I_{smxy}}{I_{pmy}}\right)^{B} - 1} + C\right] \tag{14}$$

$$t_{bxz} = TMS_{bz}\left[\frac{A}{\left(\frac{I_{sbxz}}{I_{pbz}}\right)^{B} - 1} + C\right] \tag{15}$$

where TMS_{my} and TMS_{bz} are the TMS settings of the main and the backup relays y and z respectively. Similarly, the variables I_{pmy} and I_{pbz} represent relay y and z pickup-current settings for both primary and backup operations. The fault current at location x passing through relay y in the primary operation is denoted I_{smxy} and I_{sbxz} represents the fault current at location x passing through relay z in the backup operation.

2.3.2. Coordination constraint or limit on time interval between primary and backup relay pairs

The fault current is seen by the main and the backup relay at the same instant and to avoid malfunction, the time of operation of the backup relay should be greater than that of the main relay by CTI. In cases of temporary faults, there is no need of tripping the relay, and therefore the OCRs should take a certain amount of time for its operation.

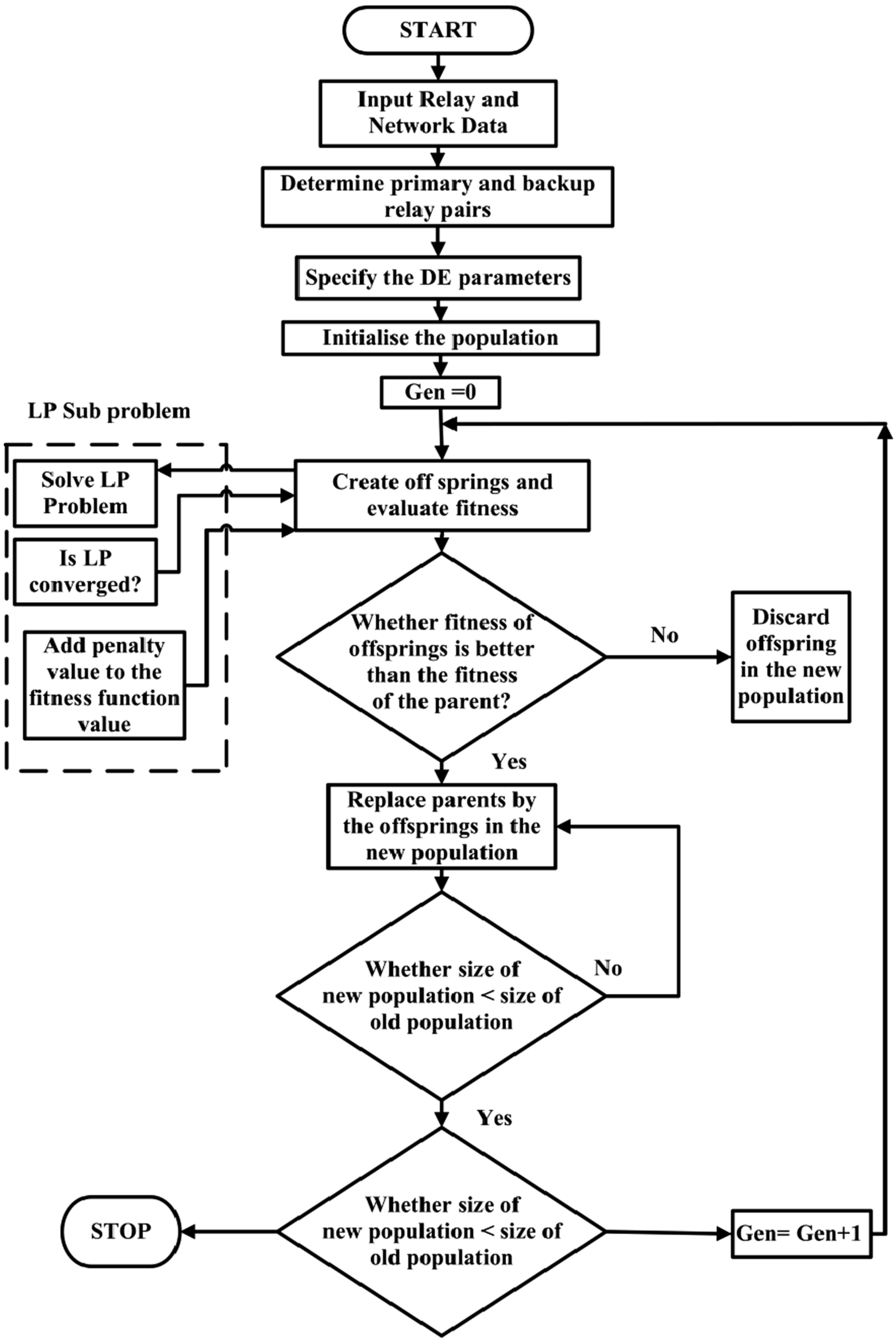

Fig. 3. Flow chart for the proposed hybrid DE-LP optimization technique.

$$t_{bxz} - t_{mxy} \geq CTI \; \forall \; y, z \tag{16}$$

2.3.3. Relay characteristics constraints

The limits for the minimum and maximum TMS values of the relays are given in Eqs. (17)–(19).

$$TMS_i^{min} \leq TMS_i \leq TMS_i^{max} \tag{17}$$

$$TMS_{my} \leq TMS_i^{min} \tag{18}$$

$$TMS_i^{max} \leq TMS_{bz} \tag{19}$$

Here TMS_i^{min} and TMS_i^{max} are the minimum and maximum value of TMS for each OCR and its value depends upon the type of relay used in the substation. The minimum plug-setting values of the relay must be greater than the maximum value of load-current and less than the minimum short-circuit current. The lower and upper limits of PS of each OCRs are calculated based on the following equations:

$$PS_i^{min} = \frac{OLFxI_{n,i}}{CTR} \tag{20}$$

$$PS_i^{max} = \frac{2xI_{f,i}^{min}}{3CTR} \tag{21}$$

where $I_{n,i}$ is the nominal current rating of the circuit protected by the

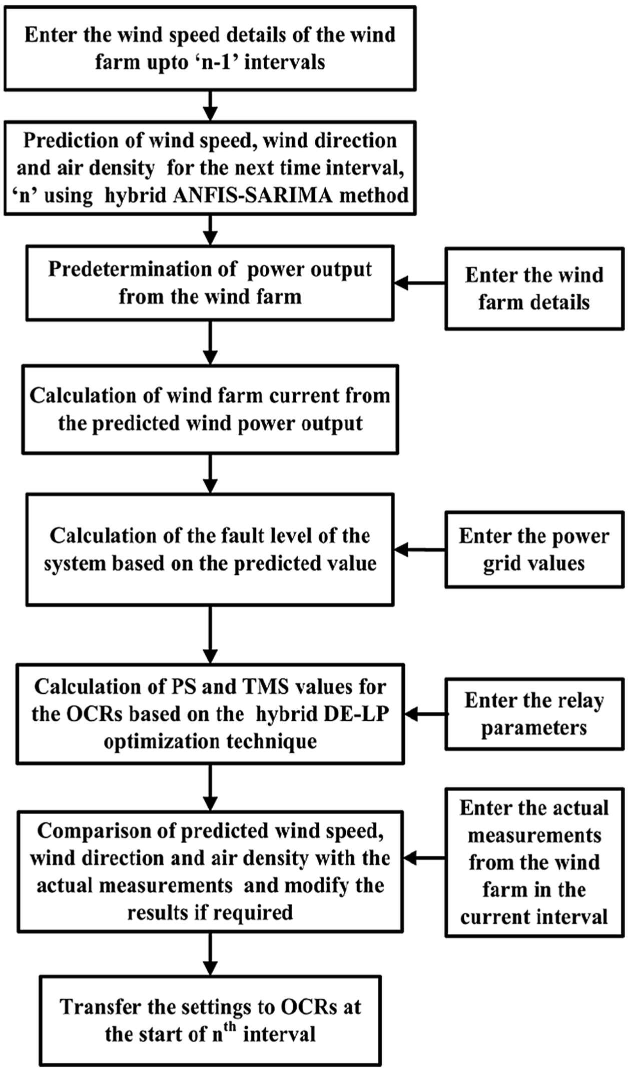

Fig. 4. Flow chart for the proposed forecast based OCR coordination (to determine the setting of the OCRs in the n^{th} interval).

relay R_i. PS_i^{min} and PS_i^{max} are the lower limit and upper limit values of PS respectively. OLF is the overload factor which is usually taken as 1.25 and $I_{f,i}^{min}$ is the minimum fault current that should be detected by the i^{th} relay.

2.4. Hybrid DE-LP algorithm for OCR coordination

The following are the steps involved in the coordination of over current relays using differential evolution algorithm. DE algorithm is an efficient evolutionary algorithm for solving numerical optimization problems based on natural selection of genes. For computation based on DE algorithm, the probabilistic distribution is not needed for generation of offspring and it takes less execution time.

2.4.1. Formulation of differential evolution algorithm

Initial population: In the first step, all parameter vector genes are imitated in the feasible range of OCR settings. The population size can be defined as *(NP, D*NR)*, where *NP* represents the number of parameter vectors, *D* is the number of control variables and NR is the total number of relays.

$$\begin{bmatrix} dial_{(1,1)} & \cdots & dial_{(1,NR)} & k_{(1,NR+1)} & \cdots & k_{(1,NR*2)} \\ \vdots & \ddots & \vdots & \vdots & \ddots & \vdots \\ dial_{(NP,1)} & \cdots & dial_{(NP,NR)} & k_{(NP,NR+1)} & \cdots & k_{(NP,NR*2)} \end{bmatrix} \tag{22}$$

Trigonometric mutation: In this step, three different vector numbers are randomly selected from the DE population for each target vector. Consider, the selected population members are $\vec{X}_{r1,G}, \vec{X}_{r2,G}, \vec{X}_{r3,G}$ for the i^{th} target vector $\vec{X}_{i,G}$. The indices r_1, r_2 and r_3 are generated only once for each mutant vector and are mutually exclusive integers randomly chosen from the range *[1,NP]*, which is also different from the index *i*. Based on Eqs. (24)–(26), three weighting coefficients are formed.

$$p' = |f(\vec{X}_{r1})| + |f(\vec{X}_{r2})| + |f(\vec{X}_{r3})| \tag{23}$$

$$P_1 = \frac{|f(\vec{X}_{r1})|}{p'} \tag{24}$$

$$P_2 = \frac{|f(\vec{X}_{r2})|}{p'} \tag{25}$$

$$P_3 = \frac{|f(\vec{X}_{r3})|}{p'} \tag{26}$$

where *f ()* is the function to be minimized. The trigonometric mutation rate *Γ* is found within the interval (0, 1) and the trigonometric mutation scheme is presented in Eqs. (27) and (28).

$$\vec{V}_{i,G+1} = \frac{\vec{X}_{r1} + \vec{X}_{r2} + \vec{X}_{r3}}{3} + (p_2 - p_1) * (\vec{X}_{r1} - \vec{X}_{r2}) + (p_3 - p_2) * (\vec{X}_{r2} - \vec{X}_{r3}) + (p_1 - p_3) * (\vec{X}_{r3} - \vec{X}_{r1}) if rand[0, 1] \le \Gamma \tag{27}$$

$$\vec{V}_{i,G+1} = \vec{X}_{r1} + F(\vec{X}_{r2} - \vec{X}_{r3}) \text{else} \tag{28}$$

where $\vec{V}_i$ is the donor vector and F is a scalar number typically found in the interval [0.4 to 1]. The parameters Γ and F are selected as 0.5 and 0.8 respectively [19].

Binomial and exponential crossover: The crossover operation is performed after creating the donor vector via mutation. This operation enhances the diversity of the population by exchanging the components of donor vector with the target vector $\vec{X}_{i,G}$ to generate the trial vector $\vec{U}_{i,G} = [\vec{U}_{1,i,G} + \vec{U}_{2,i,G} + \vec{U}_{3,i,G}, \cdots, \vec{U}_{D,i,G}]$.

Binomial crossover scheme: The binomial crossover is performed whenever a randomly generated number between 0 and 1 is less than or equal to the crossover rate C_r for each of the *D* variables. Under this condition, there will be nearly uniform distribution of number of parameters inherited from the donor vector. The binomial crossover scheme is given in Eq. (29)

$$\vec{U}_{j,i,G} = \begin{cases} \vec{V}_{j,i,G} & if\, (rand_{i,j}[0, 1] \le C_r or j = j_{rand}) \\ x_{j,i,G} otherwise \end{cases} \tag{29}$$

where $rand_{i,j}$ [0, 1] is a uniformly distributed random number. This random function is executed for each j^{th} component of the i^{th} parameter vector. Then a randomly chosen index $j_{rand} \in$ [1, 2, …,D] ensures that the trial vector $\vec{U}_{j,i,G}$ gets at least one component from the donor vector $\vec{V}_{i,G}$. The crossover operation parameter, C_r is selected as 0.5 [19].

Exponential crossover scheme: An integer *nn* and *L* are selected randomly among the numbers [1, D]. The integer *nn* denotes the starting point of the target vector from where the exchange of components with the donor vector starts, L represents the number of components of the donor vector which contributes to the target vector. The exponential crossover scheme is presented in the Eq. (30).

$$\vec{U}_{j,i,G} = \begin{cases} \vec{V}_{j,i,G} & if\, (j \ge (nn)_D and L \ge L_c) \\ x_{j,i,G} for all other j \in [1, D] \end{cases} \tag{30}$$

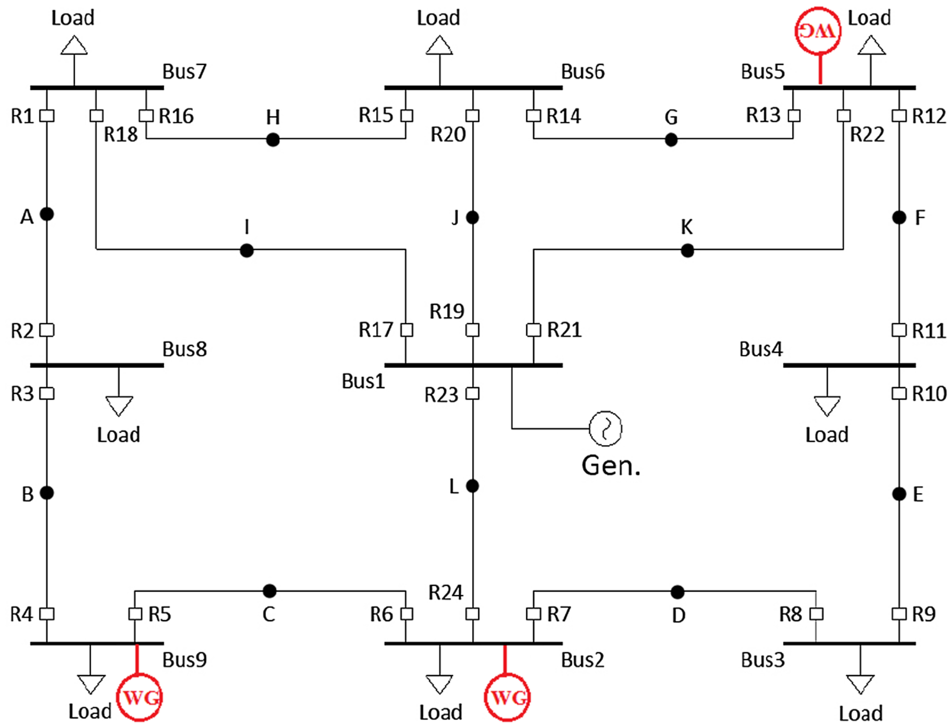

Fig. 5. Modified IEEE 9-bus system with WGs at buses 2, 5, and 9.

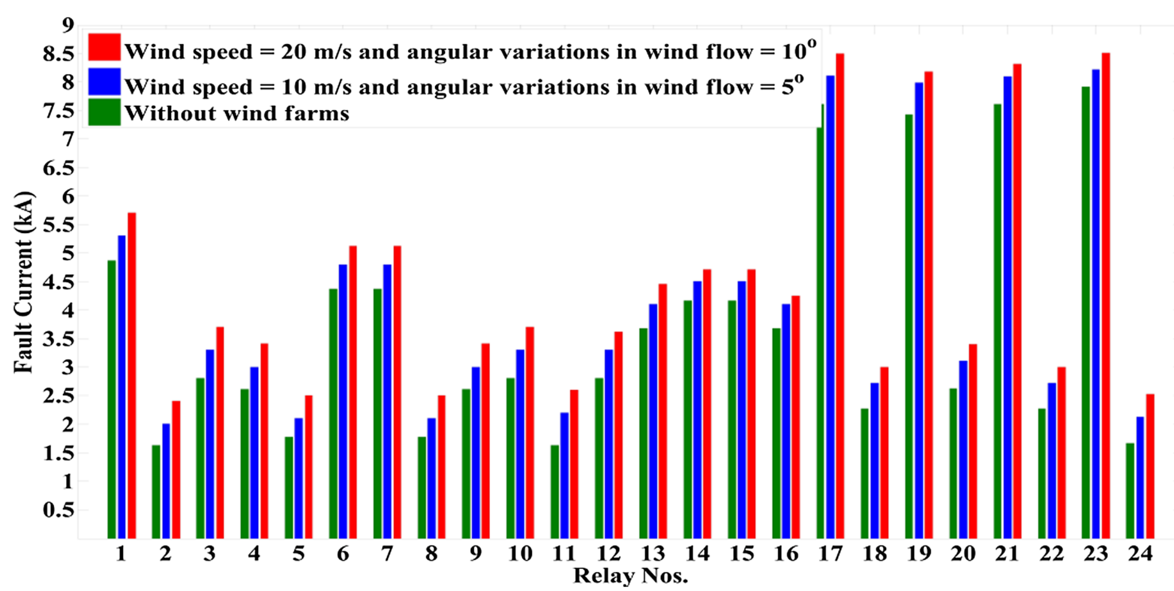

Fig. 6. Variation in fault currents seen by the main relays for the modified IEEE 9-bus system with wind farms.

here $(nn)_D$ is the starting point of crossover and L_c is the counter of L which can be initially expressed as $L_c = 0$, where $L_c = L_c + 1$ for every evaluation of j^{th} component (L ≤ D).

Selection: The selection operation determines whether the trial or the target vector gets through to the following generation. An example for the selection operation at generation $G = G + 1$ is stated below

$$\vec{X}_{i,G+1} = \begin{cases} \vec{U}_{i,j} & iff\ (\vec{U}_{i,j}) \le f(\vec{X}_{i,G}) \\ \vec{X}_{i,G} & iff\ (\vec{U}_{i,j}) > f(\vec{X}_{i,G}) \end{cases} \tag{31}$$

where $f(\vec{x})$ and $f(\vec{U})$is the fitness of the target vector and trail vector respectively. If a lower or equal value of fitness is obtained from the new trial vector, then the target vector will be replaced in the next generation; otherwise the target vector is kept in the population. By doing so, the population will never deteriorate since it either gets better or remains the same in fitness quality.

The various steps for the protection coordination using differential evolution optimization method is given below

1. Randomly generate the initial population in which each gene of the parameter vectors is found within the feasible solution for the problem.
2. Perform the trigonometric mutation.

a. For each target vector, evaluate the fitness *f(x)* of the three selected mutually exclusive parameter vectors.
b. According to the Eq. (23), calculate weighting coefficients.
c. For each target vector, create the donor vector according to Eqs.

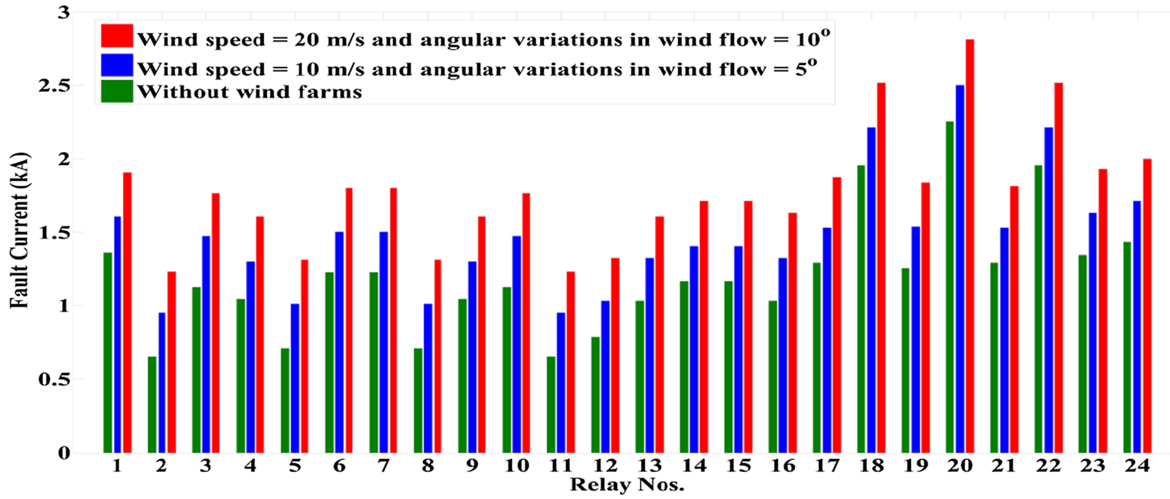

Fig. 7. Variation in fault currents seen by the backup relays for the modified IEEE 9-bus system with wind farms.

Table 1
Mal-functions in the conventional protection scheme for the modified IEEE 9-bus system.

Wind speed (m/s)	No. of violations in CTI
5	10
8	8
10	4
15	8
18	6
24	7

(27) and (28).

3. Conduct crossover mutation.
d. To form trial vectors, perform binomial or exponential crossover according to the Eqs. (29) and (30).
4. Carryout selection process.
e. For both target and trial vectors, evaluate their fitness f(x) quality.
f. Perform selection according to the equation (31), in order to generate the new population.
5. For the new population, evaluate the fitness f(x) quality.
6. Execute the algorithm anew using the new population.

Repeat all the steps from 2 to 6 and terminate until the stopping criteria is met.

The simplex method of linear programming is used for finding the optimal setting for TMS values. The primary and backup relay pairs are determined and the fault currents passing through the relays at the selected points are calculated. The PS values of the over-current relays are selected randomly within its limits and the non-linear coordination problem is converted to a linear one. The PS values randomly chosen are only for initialization in the first iteration and new PS values are determined by the DE algorithm. The LP sub-problem is called repeatedly by the main DE algorithm. Convergence of the sub-problem is checked, and a large penalty value is added to the objective function in the case of no convergence. In the main problem, the process is repeated until the algorithm converges to the optimum solution. The flow chart representation for the hybrid DE-LP algorithm for over current relay coordination is shown in Fig. 3.

The Fig. 4 shows the flow chart representation of the forecast based algorithm for avoiding the coordination problem in the OCRs. Details of the wind speed, wind direction and meteorological information are obtained over a week and these data were used for training the ANFIS for wind prediction. Short-term forecasting of the wind is used in the study. The fault current is predetermined from the predicted wind using Eqs. (10) and (11). The optimization technique used in this algorithm is hybrid DE-LP as it has better performance compared to other optimization algorithms. The difference between the operating time of the main and backup relays should be greater than CTI. If the difference is less than CTI, the optimization is carried out by increasing the number of iterations. The discrepancy between the actual and predicted fault current is checked in each interval and TMS, PS values are modified accordingly. The algorithm also compares the actual weather conditions, wind speed and wind directions and modifies the predicted power output based on the actual measurements if the error value is beyond the limit (2%). The algorithm works in a cyclic manner by updating the wind profile of the region and thereafter modifying the settings of the OCRs.

3. Case studies

An IEEE 9-bus system and a real wind-integrated substation have been taken for implementing the proposed relay coordination algorithm. The dynamic nature of wind speed and wind direction is taken into consideration and the optimal relay settings, i.e., TMS and PS values, are predicted. The objective of the optimization problem is to minimize the overall operating time of the primary and backup relays,

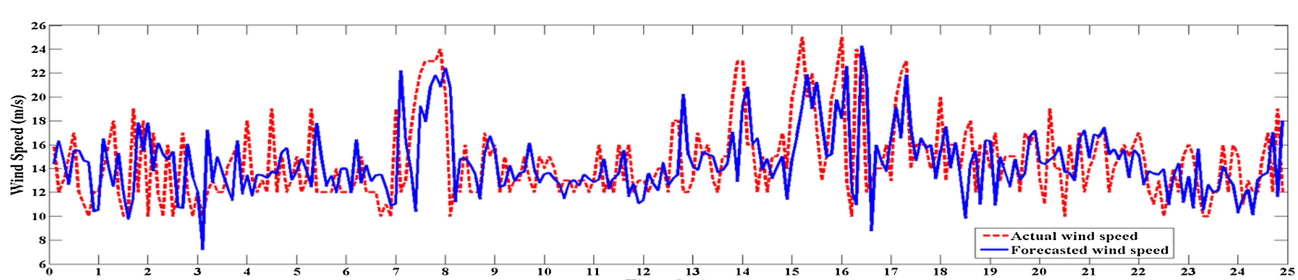

Fig. 8. Forecasted and actual wind speed for a day with an interval of five minutes.

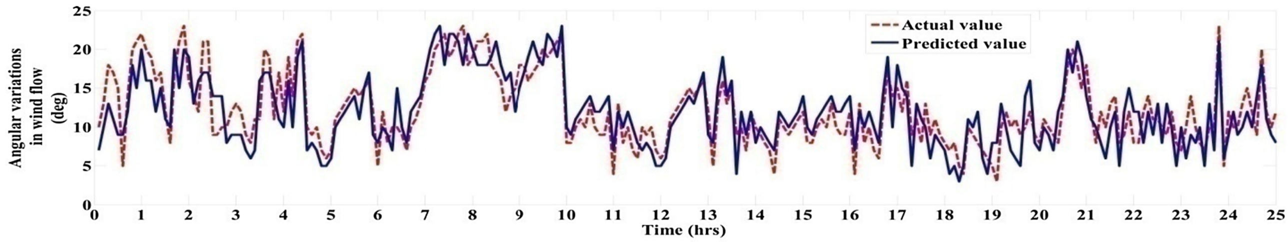

Fig. 9. Forecasted and actual wind direction for a day with an interval of five minutes.

Table 2
Error comparison of wind speed forecasting using the hybrid ANFIS-SARIMA method.

Parameters	Hybrid ANFIS-SARIMA method	
	Without considering the meteorological conditions	Considering the meteorological conditions
Error Standard Deviation	3.9218	3.8913
Mean Error	0.0640	0.0632
Mean Absolute Error (MAE)	0.9612	0.9534
Mean-Square Error (MSE)	10.4940	10.4312
Root Mean-Square Error (RMSE)	2.4523	2.3216

Table 3
Error comparison using different techniques for the wind speed prediction.

Parameters	Error Standard Deviation	Mean Error	Mean Absolute Error (MAE)	Mean-Square Error (MSE)	Root-Mean-Square Error (RMSE)
Persistence method [29]	4.7609	0.0913	1.5832	17.3216	3.5679
Support vector machine method [30]	4.5754	0.0832	1.3412	15.5413	3.2314
Extreme learning machine method [31]	4.2345	0.0764	1.3087	14.2095	3.0732
MFNN-GA method [32]	4.0234	0.0658	1.2871	12.6715	2.5632
RBFNN-GA method [32]	3.9452	0.0647	1.1074	11. 5614	2.4342
Proposed ANFIS-SARIMA hybrid method	3.8913	0.0632	0.9534	10.4312	2.3216

Table 4
Comparison of computation time required for different optimization algorithms.

Topologies	GA-LP [23]	CS-LP [22]	DE [19]	Proposed DE-LP
Without WGs	85.64	75.95	80.98	71.02
Wind speed = 10 m/s Angular variations in wind flow = 5°	87.65	77.32	82.45	72.78
Wind speed = 20 m/s Angular variations in wind flow = 10°	88.87	78.15	83.67	72.86

Table 5
Comparison of objective function value (total operating time of the OCRS) for different optimization algorithms.

Topologies	GA-LP [23]	CS-LP [22]	DE [19]	Proposed DE-LP
Without WGs	35.74	34.55	36.37	27.86
Wind speed = 10 m/s Angular variations in wind flow = 5°	37.34	35.35	38.63	28.25
Wind speed = 20 m/s Angular variations in wind flow = 10°	38.17	36.39	40.72	29.65

Table 6
Optimal TMS and PS values for the OCRs using conventional method, CS-LP hybrid method and the proposed DE-LP hybrid method (wind speed = 10 m/s and angular variation in wind flow = 5°)

Relay No.	Conventional relay settings		Hybrid CS-LP method [22]		Proposed hybrid DE-LP method	
	PS	TMS	PS	TMS	PS	TMS
1	0.6	0.14	0.5	0.14	0.5	0.11
2	1.1	0.19	0.6	0.17	0.7	0.14
3	1.2	0.18	1.0	0.18	0.8	0.12
4	0.7	0.19	0.9	0.15	0.8	0.11
5	0.7	0.17	0.8	0.17	0.6	0.12
6	1.1	0.17	1.1	0.14	0.5	0.14
7	1.0	0.16	0.7	0.14	0.7	0.12
8	0.9	0.19	0.9	0.12	0.9	0.12
9	0.8	0.18	0.7	0.12	0.5	0.11
10	0.7	0.18	0.7	0.15	0.8	0.11
11	0.6	0.15	0.5	0.14	0.5	0.12
12	0.6	0.18	0.7	0.15	0.7	0.11
13	1.2	0.17	1.0	0.17	0.8	0.12
14	1.2	0.19	0.8	0.19	0.9	0.11
15	0.9	0.17	0.7	0.16	0.5	0.15
16	0.8	0.18	0.7	0.17	0.7	0.14
17	0.8	0.19	0.6	0.15	0.5	0.12
18	0.7	0.17	0.6	0.18	0.5	0.14
19	0.8	0.18	0.7	0.16	0.7	0.16
20	0.9	0.18	0.8	0.17	0.5	0.14
21	0.7	0.18	0.6	0.15	0.6	0.13
22	0.9	0.19	0.9	0.18	0.5	0.17
23	1.0	0.18	0.8	0.17	0.6	0.15
24	0.8	0.19	0.8	0.17	0.8	0.16

Table 7
Time of operation of the main and backup relays using conventional method, CS-LP hybrid method and the proposed adaptive method (wind speed = 10 m/s and angular variation in wind flow = 5°).

Time of operation of main (M) and backup (b_1 and b_2) relays for IEEE 9-bus system (s)								
Conventional Relay Settings			Hybrid CS-LP method [22]			Proposed hybrid DE-LP method		
M	b_1	b_2	M	b_1	b_2	M	b_1	b_2
R_{1} 0.63	R_{15} 1.14	R_{17} 1.55	R_{1} 0.53	R_{15} 1.12	R_{17} 1.23	R_{1} 0.42	R_{15} 0.95	R_{17} 1.23
R_{2} 0.87	R_{4} 1.66	-	R_{2} 0.75	R_{4} 1.45	-	R_{2} 0.53	R_{4} 1.24	-
R_{3} 0.85	R_{1} 1.21	-	R_{3} 0.53	R_{1} 1.05	-	R_{3} 0.29	R_{1} 0.67	-
R_{4} 0.73	R_{6} 0.58	-	R_{4} 0.64	R_{6} 1.15	-	R_{4} 0.45	R_{6} 1.10	-
R_{5} 0.52	R_{3} 0.96	-	R_{5} 0.38	R_{3} 0.87	-	R_{5} 0.35	R_{3} 0.65	-
R_{6} 0.58	R_{8} 0.94	R_{23} 1.37	R_{6} 0.51	R_{8} 0.74	R_{23} 1.37	R_{6} 0.40	R_{8} 0.54	R_{23} 1.03
R_{7} 0.57	R_{5} 0.94	R_{23} 1.67	R_{7} 0.39	R_{5} 0.65	R_{23} 1.64	R_{7} 0.23	R_{5} 0.42	R_{23} 1.02
R_{8} 0.73	R_{10} 1.35	-	R_{8} 0.62	R_{10} 1.19	-	R_{8} 0.43	R_{10} 0.83	-
R_{9} 0.46	R_{7} 0.95	-	R_{9} 0.42	R_{7} 0.88	-	R_{9} 0.31	R_{7} 0.56	-
R_{10} 0.64	R_{12} 0.73	-	R_{10} 0.52	R_{12} 0.83	-	R_{10} 0.45	R_{12} 0.67	-
R_{11} 0.82	R_{9} 1.23	-	R_{11} 0.71	R_{9} 1.12	-	R_{11} 0.67	R_{9} 1.08	-
R_{12} 0.53	R_{14} 0.97	R_{21} 1.63	R_{12} 0.47	R_{14} 0.96	R_{21} 1.24	R_{12} 0.35	R_{14} 0.67	R_{21} 1.21
R_{13} 0.34	R_{11} 0.45	R_{21} 1.47	R_{13} 0.32	R_{11} 0.72	R_{21} 1.25	R_{13} 0.24	R_{11} 0.60	R_{21} 1.13
R_{14} 0.63	R_{16} 0.95	R_{19} 1.36	R_{14} 0.53	R_{16} 0.85	R_{19} 1.27	R_{14} 0.45	R_{16} 0.76	R_{19} 0.85
R_{15} 0.88	R_{13} 1.47	R_{19} 1.77	R_{15} 0.76	R_{13} 1.23	R_{19} 1.56	R_{15} 0.66	R_{13} 1.14	R_{19} 1.55
R_{16} 0.78	R_{2} 1.27	R_{17} 1.57	R_{16} 0.64	R_{2} 1.12	R_{17} 1.35	R_{16} 0.52	R_{2} 0.93	R_{17} 1.19
R_{17} 0.90	-	-	R_{17} 0.75	-	-	R_{17} 0.53	-	-
R_{18} 0.82	R_{2} 1.26	R_{15} 1.62	R_{18} 0.68	R_{2} 1.07	R_{15} 1.42	R_{18} 0.60	R_{2} 0.92	R_{15} 1.20
R_{19} 0.92	-	-	R_{19} 0.73	-	-	R_{19} 0.55	-	-
R_{20} 1.06	R_{13} 1.47	R_{16} 1.70	R_{20} 1.03	R_{13} 1.25	R_{16} 1.48	R_{20} 0.83	R_{13} 1.21	R_{16} 1.44
R_{21} 0.82	-	-	R_{21} 0.68	-	-	R_{21} 0.35	-	-
R_{22} 1.47	R_{11} 1.35	R_{14} 1.97	R_{22} 1.34	R_{11} 1.55	R_{14} 1.78	R_{22} 1.14	R_{11} 1.37	R_{14} 1.35
R_{23} 0.89	-	-	R_{23} 0.57	-	-	R_{23} 0.35	-	-
R_{24} 0.50	R_{5} 0.85	R_{8} 1.47	R_{24} 0.42	R_{5} 0.63	R_{8} 1.05	R_{24} 0.31	R_{5} 0.53	R_{8} 0.95

Table 8
Impact of fault resistance on total operating time of the relays in conventional and proposed approaches (wind speed = 10 m/s and angular variation in wind flow = 5°).

Fault resistance (R_f)	Hybrid GA-LP method [23]	Hybrid CS-LP method [22]	Proposed hybrid DE-LP method
0.00	36.45	34.64	27.58
0.10	37.34	35.35	28.25
0.25	37.78	36.19	28.91
0.50	38.21	36.76	29.43

subjected to the coordination constraints. The proposed algorithm is also validated through experimentation in the laboratory.

3.1. IEEE 9-Bus system

The IEEE 9-bus interconnected distribution system is taken for the validation of the proposed algorithm. It has one single-end fed by a power source of 33 kV, 100 MVA capacity at bus 1 with a source impedance of (0 + j0.1) p.u. The lines have the same impedance and it is equal to (0 + j0.2) p.u. The system has 3φ fault which is inserted at the midpoint of each line, as shown in Fig. 5. The nodes are added at the midway point of the lines (A-L) which represent the fault location where the three phase short-circuit analysis is carried out. The fault

Table 9
Overall operating time of relays considering different WG sizes and location (wind speed = 10 m/s and angular variation in wind flow = 5°).

Wind Generator size and location	Hybrid GA-LP method [23]	Hybrid CS-LP method [22]	Proposed hybrid DE-LP method
WGs of 5 MVA at bus 5 only	36.15	30.02	23.19
WGs of 3MVA at buses 5 and 2	36.49	30.98	24.24
WGs of 3 MVA at bus 5 and 5 MVA at bus 9	36.86	31.45	25.03
WGs of 5 MVA at buses 2, 5 and 9	37.34	35.35	28.25

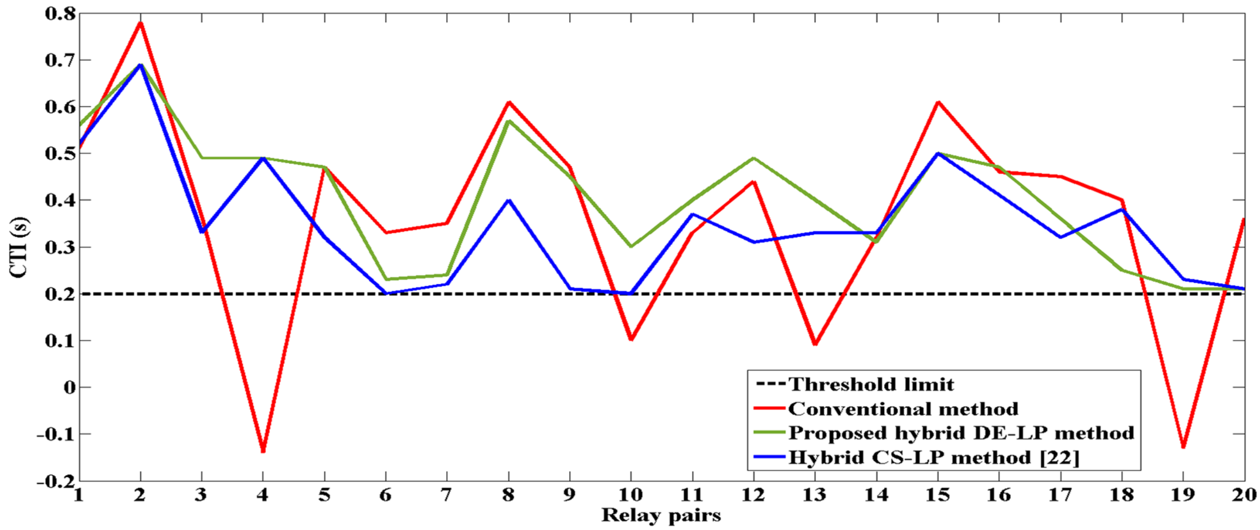

Fig. 10. CTI between the relay pairs for the modified IEEE 9-bus system with wind farms.

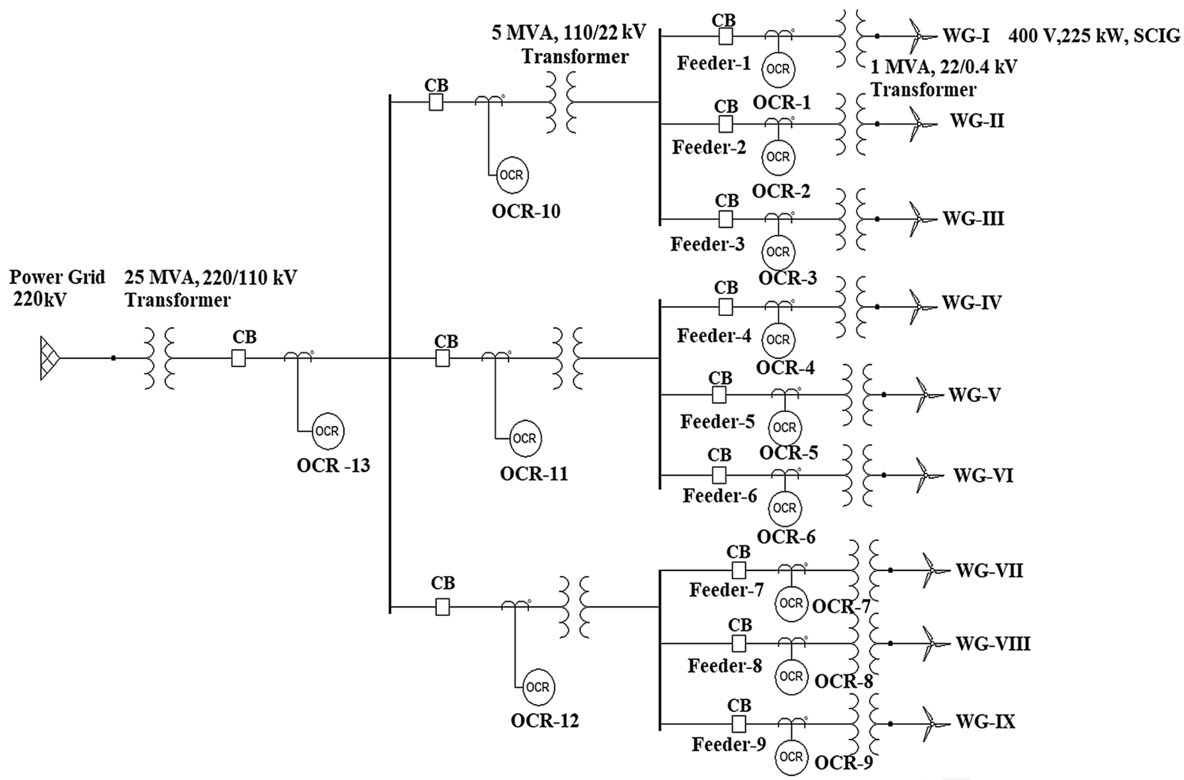

Fig. 11. Typical wind integrated substation.

Table 10
Faulty operation of OCRs reported in the substation.

Sl. No.	Fault details		Tripping status	
	Date	Fault location	Feeder breaker	Main feeder breaker
1	29/06/18	Feeder 1 fault	Not tripped	Tripped
2	03/07/18	Feeder 5 fault	Not tripped	Not tripped
3	07/07/18	Feeder 9 fault	Not tripped	Tripped

analysis is carried out using electrical transient analysis program (ETAP) software. All the OCRs have the same CT ratio of 500:1 and are considered to be numerical, in which both PS and TMS are continuous. The minimum operating time of each relay is taken as 0.2 s.

The 24 OCRs are numbered as R_1, R_2, …, R_{24} and the settings of all the relays are to be optimized for coordination. Consequently, there are 48 decision variables, i.e., TMS_1 to TMS_{24} and PS_1 to PS_{24}. The OCRs have PS values varying from 0.5 to 2 and the range of TMS is from 0.05 to 1.1. The network shown in Fig. 5 is analyzed to identify the primary and backup relay pairs using graph theory analysis. The relays R17, R19, R21 and R23 have no back up protection. In the next step, short-circuit currents measured by the main and backup relays are calculated. The pickup currents are fixed after the selection of transformer currents based on the obtained data for load flow analysis and fault currents. Then, the coordination problem is solved using optimization technique where the objective function given in Eqs. (14) and (15) is minimized by optimizing the relay parameters PS and TMS.

The variation of the fault current observed by the main and backup

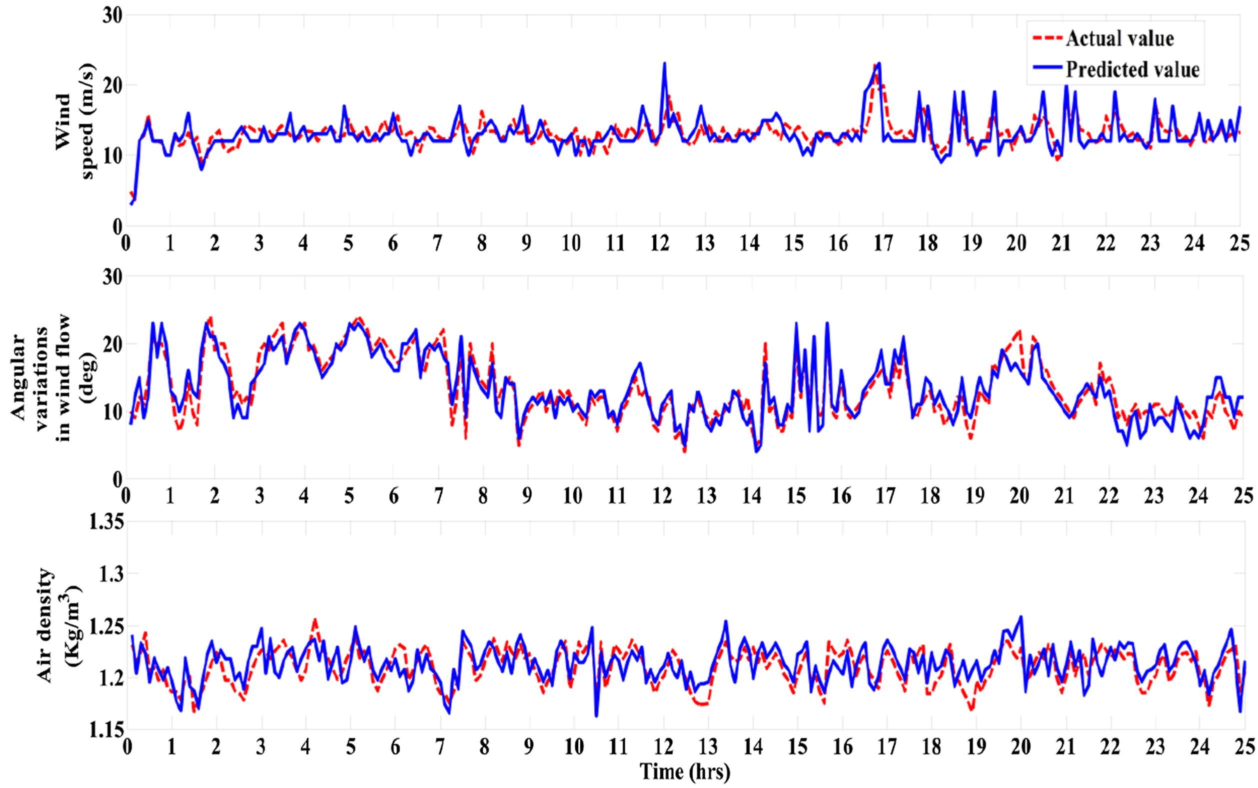

Fig. 12. The response of wind speed, wind direction and air density for a day in winter season (17/12/2018).

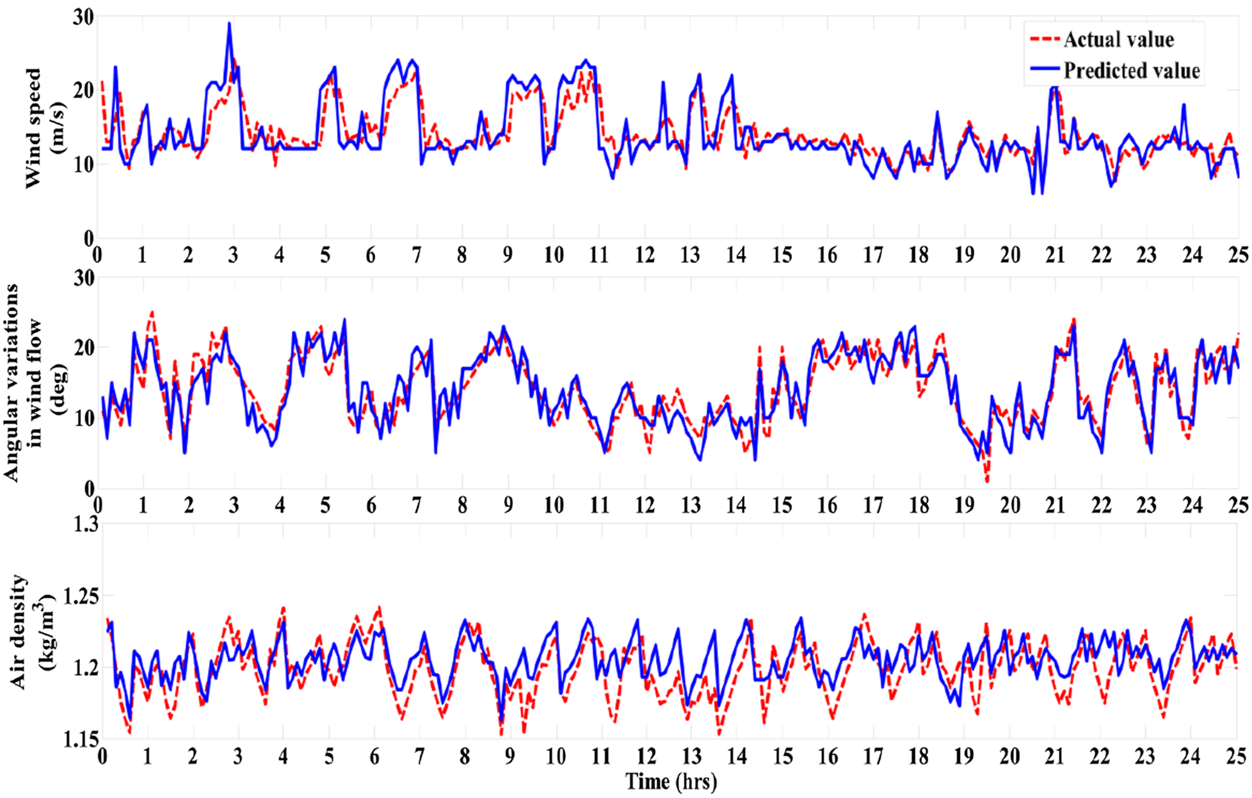

Fig. 13. The response of wind speed, wind direction and air density for a day in summer season (12/04/19).

relays in line with the dynamic nature of wind farms is given in Figs. 6 and 7. The IEEE 9-bus system is modified with an induction generator based WG unit, rated at 5 MVA and is added to buses 5, 7 and 10. It is noted that the fault current increases with an increase in wind speed and two cases (wind speed of 10 m/s and 20 m/s, with the angular variation of 5° and 10° respectively) have been taken into consideration. The conventional relay settings for the IEEE 9-bus system are based without the integration of any DG sources to it. If the same settings are

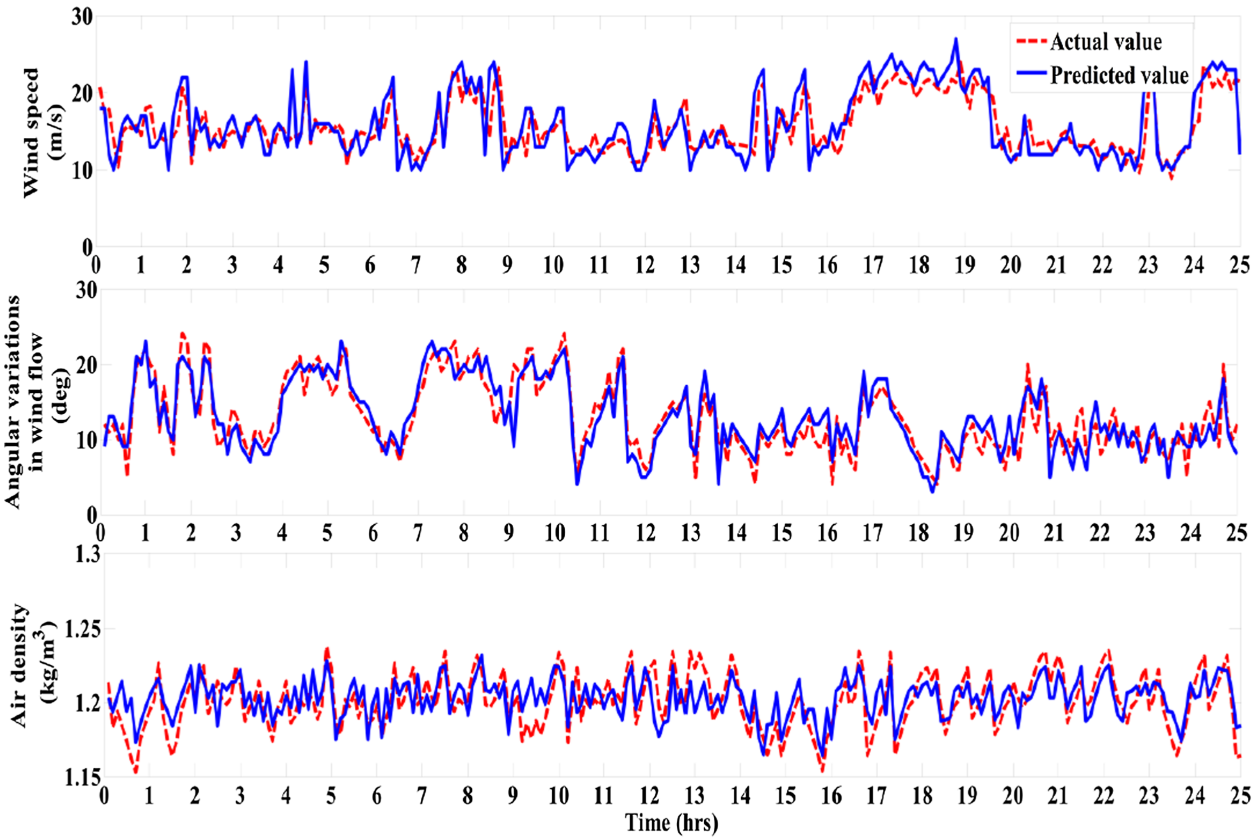

Fig. 14. The response of wind speed, wind direction and air density for a day in monsoon season (29/06/19).

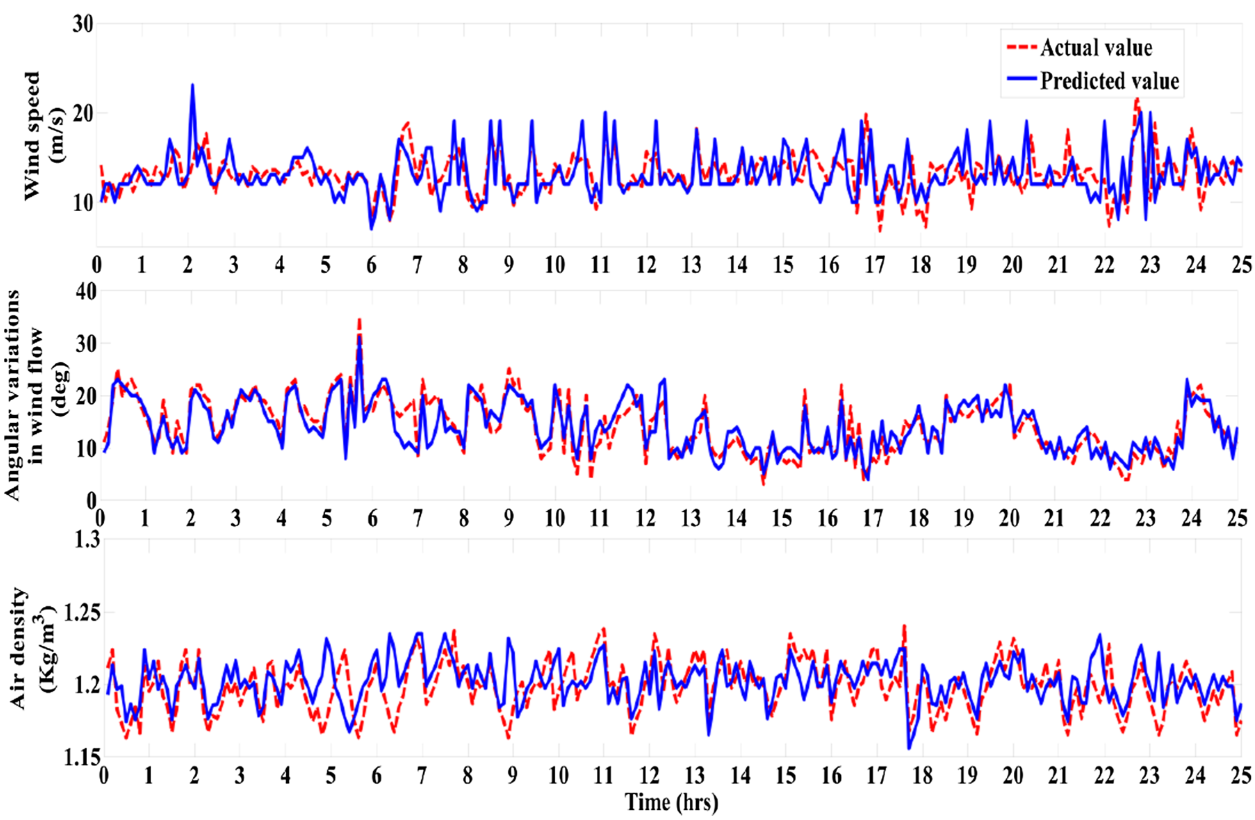

Fig. 15. The response of wind speed, wind direction and air density for a day in autumn season (08/09/2019).

Table 11
PS and TMS values for the OCRs in a typical wind integrated substation (wind speed = 10 m/s and angular variation in wind flow = 5°).

OCR No.	Existing settings		Hybrid CS-LP method [22]		Proposed DE-LP method	
	PS	TMS	PS	TMS	PS	TMS
1	0.6	0.12	0.4	0.12	0.4	0.10
2	1.2	0.19	0.6	0.16	0.9	0.13
3	1.0	0.17	0.8	0.19	0.7	0.14
4	0.6	0.19	0.6	0.13	0.8	0.13
5	0.7	0.17	0.9	0.18	0.7	0.11
6	1.2	0.16	1.1	0.14	0.5	0.10
7	0.9	0.14	0.8	0.15	0.8	0.14
8	0.7	0.19	0.7	0.12	0.7	0.11
9	0.6	0.18	0.5	0.11	0.6	0.12
10	0.8	0.15	0.6	0.13	0.8	0.10
11	0.6	0.15	0.5	0.18	0.5	0.12
12	0.8	0.19	0.6	0.15	0.6	0.11
13	1.3	0.17	0.9	0.16	0.8	0.10

used for the system with the wind farm, miscoordination between main and backup relays will occur, which results in the faulty operation of the relays.

The wind speed is varied between 5 m/s and 25 m/s which results in the change of fault current from wind farm. So, the CTI is not always maintained between primary and secondary relays. The number of violations in CTI with the wind turbine generators working under different speed conditions is given in Table 1. Therefore, the settings of the relay need to be modified according to fault level which in turn depends on the wind power output. This ensures the operation of the OCRs in the system without any time delay when a fault occurs in the system. The azimuthal angular variation in the wind flow is taken as 5° for all the cases given in the Table 1.

The prediction of the wind speed and wind direction is carried out using the hybrid ANFIS-SARIMA method. In most of the WGs, the cut-in speed is taken as 5 m/s and the cut-out speed is taken as 25 m/s. The wind speed at the wind farm is varied between 5 m/s and 25 m/s and the azimuthal angular variations in the wind flow are taken in the range of 0° to 25°. The data set of 2016 samples is used for training the hybrid ANFIS-SARIMA method for both wind speed and wind direction. The short-term forecasting for the wind is performed at five-minute intervals. The following graph (Figs. 8 and 9) shows the predicted wind speed and wind direction for one day at five-minute intervals. Thus, the wind-farm current is calculated using the predicted wind speed and wind direction and the relay settings are fixed using the DE-LP hybrid optimization algorithm. The following table (Table 2) gives the comparison of wind speed forecasting with and without taking the meteorological conditions. Table 3 shows the comparison of wind speed predictions using the persistence method [29], support vector machine method [30], extreme learning machine method [31], hybrid multi feedforward neural network (MFNN) - GA method [32], hybrid radial basis function neural network (RBFNN)- GA method [32], with the proposed hybrid ANFIS-SARIMA method. The results show that the proposed hybrid method has less error compared to the methods which are already reported.

The optimization method selected in this study is the hybrid DE-LP method, and the simulation parameters for the DE-LP algorithm are given in Appendix. A comparison between the different algorithms is given in Tables 4 and 5. The computation time required for the hybrid DE-LP algorithm is less than the hybrid GA-LP, CS-LP and DE algorithms. The proposed hybrid DE-LP algorithm gives better objective function value or the reduced operating time for the relays compared to other optimization techniques.

The PS and TMS values for all the OCRs are optimized using DE-LP hybrid method and the results are given in Table 6. The optimal operating time of the primary and backup relays using the conventional method, CS-LP hybrid method and the proposed adaptive method is shown in Table 7. The selected wind speed is 10 m/s. In the conventional approach, there are some cases where the primary and back up relays did not maintain the CTI of 0.2 s which are highlighted in Table 7. For a fault at location B, R4 is the main relay and R6 is the backup relay with operating time of 0.73 s and 0.58 s respectively (with CTI of −0.15 s). In this condition, R6 operates faster than R4. Using the conventional strategy, the operating time of the primary relays are 17.94 s and that of the secondary relays are 21.73 s. The Table 7 also gives the operating time of the main and backup relays after implementing the hybrid CS-LP overcurrent relay coordination method. The sum of the primary relay operating time is 14.92 s and that of the secondary relay operating time is 20.43 s with minimum CTI for all fault conditions [22]. However, by adopting the proposed optimization

Table 12
Operating time of the main and backup relays in a typical wind integrated substation (wind speed = 10 m/s and angular variation in wind flow = 5°).

Time of operation for the main (M) and backup (b_1 and b_2) relays in a typical wind integrated system (s)								
Conventional relay Settings			Hybrid CS-LP method [22]			Proposed hybrid DE-LP method		
M	b_1	b_2	M	b_1	b_2	M	b_1	b_2
R_1 0.74	R_{10} 1.08	R_{13} 1.37	R_1 0.68	R_{10} 0. 93	R_{13} 1.35	R_1 0.58	R_{10} 0.82	R_{13} 1.02
R_2 0.94	R_{10} 1.28	R_{13} 1.70	R_2 0.88	R_{10} 1.27	R_{13} 1.62	R_2 0.72	R_{10} 0.99	R_{13} 1.35
R_3 0.85	R_{10} 0.67	R_{13} 1.63	R_3 0.75	R_{10} 0.96	R_{13} 1.37	R_3 0.65	R_{10} 0.91	R_{13} 1.26
R_4 0.73	R_{11} 1.04	R_{13} 1.31	R_4 0.66	R_{11} 0 .88	R_{13} 1.17	R_4 0.51	R_{11} 0.88	R_{13} 1.35
R_5 0.69	R_{11} 0.92	R_{13} 1.41	R_5 0.49	R_{11} 0.82	R_{13} 1.12	R_5 0.38	R_{11} 0.67	R_{13} 0.95
R_6 0.75	R_{11} 1.14	R_{13} 1.34	R_6 0.69	R_{11} 1.10	R_{13} 1.52	R_6 0.59	R_{11} 0.89	R_{13} 1.17
R_7 0.57	R_{16} 0.92	R_{22} 1.32	R_9 0.58	R_{16} 0.88	R_{22} 1.34	R_7 0.52	R_{16} 0.74	R_{22} 0.99
R_8 0.59	R_{12} 0.61	R_{13} 1.35	R_8 0.57	R_{12} 0.82	R_{13} 1.15	R_8 0.52	R_{12} 0.83	R_{13} 1.21
R_9 0.64	R_{12} 0.89	R_{13} 1.28	R_9 0.43	R_{12} 0.80	R_{13} 1.13	R_9 0.43	R_{12} 0.72	R_{13} 0.95
R_{10} 0.62	R_{13} 0.98	-	R_{10} 0.50	R_{13} 0.94	-	R_{10} 0.43	R_{13} 0.72	-
R_{11} 0.92	R_{13} 1.37	-	R_{11} 0.45	R_{13} 0.73	-	R_{11} 0.35	R_{13} 0.70	-
R_{12} 0.63	R_{13} 0.53	-	R_{12} 0.38	R_{13} 0.70	-	R_{12} 0.42	R_{13} 0.74	-

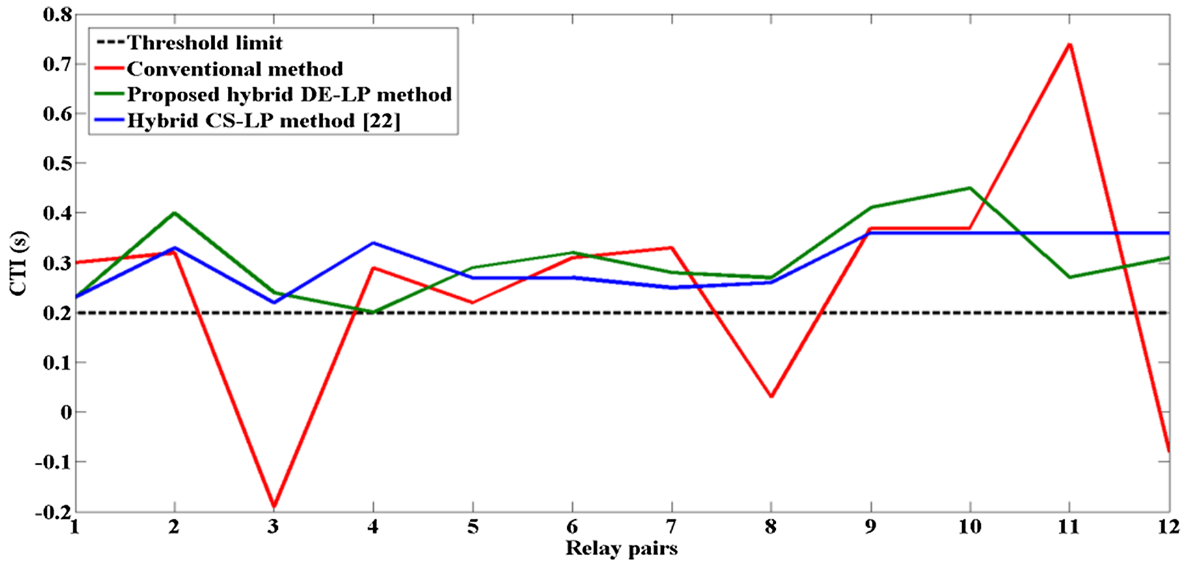

Fig. 16. CTI between the relay pairs for the typical wind integrated system.

Fig. 17. Feeder protection unit.

algorithm the operating time of the main and the backup relay are further reduced to 11.41 s and 16.84 s respectively.

The Table 8 shows the sum of the operating time of the main relay and backup relays according to the variation in the fault resistance. The results show that the proposed GA-LP approach has better performance compared to the conventional, CS-LP hybrid and GA-LP methods. The proposed algorithm was also tested using WGs of different capacities, placed at different locations. The results (Table 9) show that the proposed algorithm can be applied with any wind farms of different capacities at various locations.

The CTI for the OCRs after connecting wind farm to the grid is shown in Fig. 10. The minimum value of the CTI to be maintained is 0.2 s and this is represented as the threshold line. There are 20 co-ordination pairs in IEEE 9-bus system and results show that the CTI is not maintained for some of the relay pairs using the conventional method. This causes malfunctions in the relay operations and the algorithm was modified according to the varying wind speed conditions. The CTI is maintained and the results are found to be satisfactory.

3.2. Wind integrated substation

A typical wind farm-connected substation is also used for the case study and details are given in [33,34]. The substation has 9 feeders to which WGs are connected. Each WG is associated with a step up transformer of 1 MVA capacity which step up the generated voltage of 400 V to 22 kV. The feeders are connected to the 220 kV side using a transformer of 25 MVA and three transformers of 5 MVA which step up the 22 kV voltage to 110 kV. The fault level for 110 kV, 220 kV side of the substation is 2806 MVA and 4708 MVA. The layout of the substation is shown in Fig. 11.

The WG units significantly contribute to short-circuit currents and the connections or disconnections of WG units have considerable short-term impacts on the fault current magnitude. Large-scale wind turbine units are usually equipped with asynchronous generators that transiently draw high currents at the time of connection to the system. In case study, the generation of electric power from the wind is more dominant during the months July to November, i.e., the monsoon season. Many faulty operations of OCRs were reported during this period [33], and details of these are given in Table 10. The OCR in the

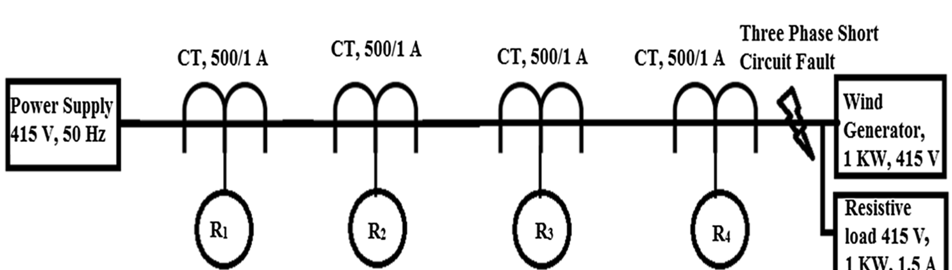

Fig. 18. Radial feeder connected to wind generator.

Table 13
TMS for the OCRs in the radial feeder protection unit.

Time interval (2:00–3:00 pm)	Wind speed predicted (m/s)	Angular variations in wind flow predicted (deg)	Wind speed measured (m/s)	Angular variations in wind flow measured (deg)	Simulated/Predicted results transferred to the relay module				Actual results			
					Relay No.				Relay No.			
					R_4	R_3	R_2	R_1	R_4	R_3	R_2	R_1
2:00	6.5	5	6.9	4	0.25	0.57	0.89	0.95	0.29	0.62	0.95	0.98
2:05	8.3	7	7.9	8	0.35	0.63	0.92	1.02	0.35	0.83	0.95	1.03
2:10	9.4	10	9.7	12	0.27	0.82	0.93	1.04	0.43	0.63	0.98	1.04
2:15	10.2	8	9.6	9	0.34	0.62	0.93	0.96	0.30	0.33	0.89	0.99
2:20	11.5	7	11.0	6	0.36	0.34	1.02	0.97	0.29	0.35	0.95	1.16
2:25	14.6	12	14.3	11	0.43	0.45	0.99	1.15	0.42	0.42	0.99	1.14
2:30	12.5	14	12.1	12	0.30	0.42	0.98	1.12	0.33	0.46	0.87	1.03
2:35	9.9	11	9.1	11	0.25	0.40	0.92	0.97	0.42	0.54	0.84	1.07
2:40	13.5	12	12.9	11	0.35	0.49	0.88	1.03	0.32	0.60	0.83	1.15
2:45	14.4	8	15.0	8	0.40	0.44	0.83	1.10	0.34	0.64	0.85	1.06
2:50	5.4	6	5.1	5	0.38	0.60	0.89	1.16	0.36	0.70	0.86	1.18
2:55	7.7	6	8.2	5	0.25	0.72	0.78	1.14	0.32	0.72	0.84	0.99
3:00	11.6	2	12.0	3	0.29	0.64	0.79	1.20	0.27	0.77	0.79	1.20

Table 14
PS for the OCRs in the radial feeder protection unit.

Time interval (2:00–3:00 pm)	Wind speed predicted (m/s)	Angular variations in wind flow predicted (deg)	Wind speed measured (m/s)	Angular variations in wind flow measured (deg)	Simulated/Predicted results				Actual results			
					Relay No.				Relay No.			
					R_4	R_3	R_2	R_1	R_4	R_3	R_2	R_1
2:00	6.5	5	6.9	4	0.72	0.65	0.62	0.57	0.73	0.62	0.64	0.53
2:05	8.3	7	7.9	8	0.77	0.72	0.68	0.62	0.75	0.62	0.58	0.33
2:10	9.4	10	9.7	12	0.78	0.67	0.63	0.58	0.75	0.64	0.62	0.35
2:15	10.2	8	9.6	9	0.77	0.72	0.66	0.62	0.77	0.64	0.53	0.33
2:20	11.5	7	11.0	6	0.66	0.62	0.56	0.52	0.82	0.69	0.53	0.56
2:25	14.6	12	14.3	11	0.72	0.62	0.57	0.52	0.75	0.72	0.56	0.62
2:30	12.5	14	12.1	12	0.71	0.66	0.63	0.56	0.77	0.63	0.56	0.53
2:35	9.9	11	9.1	11	0.73	0.68	0.62	0.57	0.78	0.62	0.57	0.51
2:40	13.5	12	12.9	11	0.72	0.65	0.59	0.56	0.69	0.63	0.58	0.53
2:45	14.4	8	15.0	8	0.69	0.64	0.56	0.55	0.68	0.62	0.55	0.53
2:50	5.4	6	5.1	5	0.68	0.62	0.54	0.53	0.66	0.59	0.55	0.53
2:55	7.7	6	8.2	5	0.66	0.59	0.55	0.52	0.65	0.58	0.53	0.52
3:00	11.6	2	12.0	3	0.65	0.57	0.53	0.50	0.64	0.57	0.53	0.52

Table 15
Operating time of the main and back up relays in the radial feeder protection unit.

Time interval (2:00–3:00 pm)	Wind speed predicted (m/s)	Wind direction predicted (deg)	Wind speed measured (m/s)	Wind direction measured (deg)	Simulated/Predicted results				Actual results			
					Relay No.				Relay No.			
					R_4	R_3	R_2	R_1	R_4	R_3	R_2	R_1
2:00	6.5	5	6.9	4	1.46	1.68	1.92	2.15	1.47	1.68	1.92	2.13
2:05	8.3	7	7.9	8	1.52	1.74	1.96	2.15	1.55	1.76	1.97	2.18
2:10	9.4	10	9.7	12	1.52	1.73	1.95	2.15	1.54	1.75	1.97	2.18
2:15	10.2	8	9.6	9	1.52	1.78	1.99	2.20	1.53	1.79	2.02	2.24
2:20	11.5	7	11.0	6	1.71	1.92	2.15	2.42	1.72	1.97	2.20	2.46
2:25	14.6	12	14.3	11	1.91	2.12	2.32	2.54	1.93	2. 17	2.42	2.50
2:30	12.5	14	12.1	12	1.85	2.04	2.27	2.47	1.80	1.98	2.21	2.50
2:35	9.9	11	9.1	11	1.52	1.75	2.07	2.27	1.48	1.78	2.09	2.32
2:40	13.5	12	12.9	11	1.48	1.69	1.89	2. 23	1.52	1.67	1.86	2.19
2:45	14.4	8	15.0	8	1.57	1.80	1.94	2.35	1.56	1.80	1.83	2.52
2:50	5.4	6	5.1	5	1.67	1.87	2.16	2.45	1.62	1.83	2.14	2.42
2:55	7.7	6	8.2	5	1.74	1.97	2.25	2.47	1.73	2.02	2.27	2.48
3:00	11.6	2	12.0	3	1.56	1.75	1.97	2.22	1.54	1.78	1.97	2.23

main feeder, i.e., the backup relay, is tripped by faults in the wind farm feeders and thus the reliability of the system is affected. The time series graph for the actual and predicted wind speed, wind direction and air density for a typical day in winter, summer, monsoon and autumn seasons with an interval of five minutes are shown in Figs. 12–15.

The proposed algorithm is implemented in the system and the modified relay settings according to the variation in the wind power output are determined. The TMS and PS values for all the relays using the existing method, hybrid CS-LP [22], proposed DE-LP method for a particular interval is given in Table 11 and the operating time of the relays are given in Table 12. The result shows that the proposed algorithm has reduced time of operation of the relays by maintaining the

CTI and also avoids the computational time required for the algorithm by the earlier prediction of the relay settings.

The computation time for running the forecasting algorithm is 70 s and that for the optimization algorithm is 80 s. The computation time for the optimization is reduced in the proposed methodology by the earlier prediction of the relay settings. The proposed optimization algorithm needs to run in the current interval only if the difference between the predicted and the actual wind farm currents are above 2%. This happens very rare and the time required for optimization in the existing algorithms is reduced by the earlier setting of the relays, at the starting of each five minutes interval.

The CTI results for the different optimization techniques are shown in Fig. 16. The minimum value of the CTI to be maintained is 0.2 s and this is represented as the threshold line. There are 12 coordination pairs and results show that the CTI is not maintained for some of the relay pairs by using the existing relay settings in the substation. This causes mal-functions in the OCRs and the relay settings are modified according to the varying wind speed conditions. The CTI is maintained by using the proposed algorithm and the results are found to be acceptable.

4. Validation of the proposed algorithm in the laboratory

The proposed algorithm for OCR relay coordination is tested and verified through experimentation in the laboratory (Fig. 17). The experimental setup consists of a radial feeder protection unit with four OCRs. The type of the relays used is MC31A manufactured by L&T [35] with normal inverse characteristics. The configuration of the feeder and the OCRs is shown in Fig. 18. The main relay is denoted by R_1 and the backup relays are R_2, R_3, R_4. A WG and a loading rheostat with rated capacity of 1 kW each is connected as the load. The proposed algorithm is coded into a Raspberry Pi chip [36] and wind speed is predicted at intervals of five minutes. In the next step, the optimal settings for the TMS and PS are calculated for various wind speed conditions. In order to avoid coordination problems in the OCRs, the modified settings are updated in the relay modules. The experiment is carried out under various wind speed and wind direction conditions under constant temperature and pressure. The operating time of the relays are found to be satisfactory by maintaining a CTI of 0.2 s.

The TMS and the PS values are predetermined for a particular day (03/05/2019 from 2:00 pm to 3:00 pm) and the results are given in Tables 13 and 14 respectively. The time of operation of the OCRs is also calculated and the results are given in Table 15. The predicted results are also compared with the actual results and it is found to be satisfactory avoiding the faulty operation of OCRs.

5. Conclusion

A forecast based optimization algorithm for deciding the accurate settings of the OCRs and its coordination with other OCRs in the wind integrated system is the main theme of this research work. The proposed technique calculates PS and TMS values of OCRs from the predicted wind farm current under the dynamic conditions of wind farms including the variation in wind speed and its direction. The proposed ANFIS-SARIMA hybrid algorithm for forecasting the wind parameters has less error in the output compared to the existing algorithms. The relay coordination is carried out via hybrid DE-LP optimization technique, which has better performance than conventional algorithms. The relay settings are predicted at intervals of five minutes each, which can reduce the time delay in calculating and updating the settings in the present interval for which protection is required. This can avoid the faulty relay operations reported in the substations. The algorithm was tested on the modified IEEE 9-bus system with wind farms and also in a typical wind-integrated substation. The results show that the proposed algorithm selects the optimal relay settings according to the various wind power conditions within a definite period of time. The method is also verified through experimentation in the laboratory and the results are found to be satisfactory.

CRediT authorship contribution statement

Sujo P. George: Methodology, Software, Formal analysis, Investigation, Data curation, Writing - original draft, Visualization. **S. Ashok:** Conceptualization, Validation, Resources, Writing - review & editing, Supervision, Project administration.

Declaration of Competing Interest

The authors declare that they have no known competing financial interests or personal relationships that could have appeared to influence the work reported in this paper.

Acknowledgement

The authors thank the Electrical Engineering Department of National Institute of Technology Calicut and Kerala State Electricity Board Limited (KSEB Ltd.) for the support given in conducting the research.

Appendix A

See Table A1

Table A1
Simulation parameters for the proposed hybrid DE-LP algorithm.

Differential evolution algorithm	
Maximum number of iterations	2000
Population size	100
Lower bound of scaling factor	0.2
Upper bound of scaling factor	0.8
Cross over probability	0.1
Linear programming	
Maximum iterations	100
Function tolerance	1e-6

References

[1] Dupont E, Koppelaar R, Jeanmart H. Global available wind energy with physical and energy return on investment constraints. Appl Energy 2018;209:322–38. https://doi.org/10.1016/j.apenergy.2017.09.085.

[2] Gertmar L, Liljestrand L, Lendenmann H. Wind energy powers-that-be successor generation in globalization. IEEE Trans Energy Convers 2007;22:13–28. https://doi.org/10.1109/TEC.2006.889601.

[3] Ikegami T, Urabe CT, Saitou T, Ogimoto K. Numerical definitions of wind power output fluctuations for power system operations. Renew Energy 2018;115:6–15. https://doi.org/10.1016/j.renene.2017.08.009.

[4] Mozina CJ. Impact of smart grids and green power generation on distribution systems. IEEE Trans Ind Appl 2013;49:1079–90. https://doi.org/10.1109/TIA.2013.2253292.

[5] Conti S. Analysis of distribution network protection issues in presence of dispersed generation. Electr Power Syst Res 2009;79:49–56. https://doi.org/10.1016/j.epsr.2008.05.002.

[6] Srivastava A, Tripathi JM, Krishan R, Parida SK. Optimal coordination of overcurrent relays using gravitational search algorithm with DG penetration. IEEE Trans Ind Appl 2018;54:1155–65. https://doi.org/10.1109/TIA.2017.2773018.

[7] Dubey RK, Samantaray SR, Panigrahi BK. Adaptive distance relaying scheme for transmission network connecting wind farms. Electr Power Components Syst 2014;42:1181–93. https://doi.org/10.1080/15325008.2014.921953.

[8] Singh M, Panigrahi BK, Abhyankar AR. Optimal coordination of directional overcurrent relays using Teaching Learning-Based Optimization (TLBO) algorithm. Int J Electr Power Energy Syst 2013;50:33–41. https://doi.org/10.1016/j.ijepes.2013.02.011.

[9] Sharifian H, Abyaneh HA, Salman SK, Mohammadi R, Razavi F. Determination of the minimum break point set using expert system and genetic algorithm. IEEE Trans Power Deliv 2010;25:1284–95. https://doi.org/10.1109/TPWRD.2010.2043999.

[10] Damborg MJ, Ramaswami R, Venkata SS, Postforoosh JM. Computer aided transmission protection system design. Part I: Algorithms. IEEE Trans Power Appar Syst 1984;PAS- 103:51–9. https://doi.org/10.1109/TPAS.1984.318576.

[11] Ezzeddine M, Kaczmarek R, Iftikhar MU. Coordination of directional overcurrent relays using a novel method to select their settings. IET Gener Transm Distrib 2011;5:743–50. https://doi.org/10.1049/iet-gtd.2010.0603.

[12] Razavi F, Abyaneh HA, Al-Dabbagh M, Mohammadi R, Torkaman H. A new comprehensive genetic algorithm method for optimal overcurrent relays coordination. Electr Power Syst Res 2008;78:713–20. https://doi.org/10.1016/j.epsr.2007.05.013.

[13] Urdaneta AJ, Mrquez S. Coordination of directional overcurrent relay timing using linear programming. IEEE Trans. Power Deliv 1996;11:122–9. https://doi.org/10.1109/61.484008.

[14] Chattopadhyay B, Sachdev MS, Sidhu TS. An on-line relay coordination algorithm for adaptive protection using linear programming technique. IEEE Trans. Power Deliv 1996;11:165–73. https://doi.org/10.1109/61.484013.

[15] Farzinfar M, Jazaeri M, Razavi F. A new approach for optimal coordination of distance and directional over-current relays using multiple embedded crossover PSO. Int J Electr Power Energy Syst 2014;61:620–8. https://doi.org/10.1016/j.ijepes.2014.04.001.

[16] Urdaneta AJ, Nadira R, Perez Jimenez LG. Optimal coordination of directional overcurrent relays in interconnected power systems. IEEE Trans. Power Deliv 1988;3:903–11. https://doi.org/10.1109/61.193867.

[17] Bedekar PP, Bhide SR. Expert Systems with Applications Optimum coordination of overcurrent relay timing using continuous genetic algorithm. Expert Syst Appl 2011;38:11286–92. https://doi.org/10.1016/j.eswa.2011.02.177.

[18] Zeineldin HH, El-Saadany EF, Salama MMA. Optimal coordination of overcurrent relays using a modified particle swarm optimization. Electr Power Syst Res 2006;76:988–95. https://doi.org/10.1016/j.epsr.2005.12.001.

[19] Shih MY, Conde Enríquez A, Hsiao TY, Torres Treviño LM. Enhanced differential evolution algorithm for coordination of directional overcurrent relays. Electr Power Syst Res 2017;143:365–75. https://doi.org/10.1016/j.epsr.2016.09.011.

[20] Shih MY, Castillo Salazar CA, Conde Enríquez A. Adaptive directional overcurrent relay coordination using ant colony optimisation. IET Gener Transm Distrib 2015;9:2040–9. https://doi.org/10.1049/iet-gtd.2015.0394.

[21] Alam MN, Das B, Pant V. An interior point method based protection coordination scheme for directional overcurrent relays in meshed networks. Int J Electr Power Energy Syst 2016;81:153–64. https://doi.org/10.1016/j.ijepes.2016.02.012.

[22] Dehghanpour E, Kazemi Karegar H, Kheirollahi R, Soleymani T. Optimal coordination of directional overcurrent relays in microgrids by using cuckoo-linear optimization algorithm and fault current limiter. IEEE Trans Smart Grid 2018;9:1365–75. https://doi.org/10.1109/TSG.2016.2587725.

[23] Noghabi AS, Sadeh J, Mashhadi HR. Considering different network topologies in optimal overcurrent relay coordination using a hybrid GA. IEEE Trans Power Deliv 2009;24:1857–63. https://doi.org/10.1109/TPWRD.2009.2029057.

[24] Khosravi A, Koury RNN, Machado L, Pabon JJG. Prediction of wind speed and wind direction using artificial neural network, support vector regression and adaptive neuro-fuzzy inference system. Sustain Energy Technol Assessments 2018;25:146–60. https://doi.org/10.1016/j.seta.2018.01.001.

[25] Zhang J, Wei YM, Tan ZF, Wang K, Tian W. A hybrid method for short-term wind speed forecasting. Sustain 2017;9:596. https://doi.org/10.3390/su9040596.

[26] Choukulkar A, et al. A new formulation for rotor equivalent wind speed for wind resource assessment and wind power forecasting. Wind Energ 2016;19:1439–52. https://doi.org/10.1002/we.1929.

[27] IEEE PES Joint Working Group: 'Fault Current Contributions from Wind Plants' 2013.

[28] Das S, Santoso S. Effect of wind speed variation on the short-circuit contribution of a wind turbine. IEEE Power Energy Soc Gen Meet, IEEE 2012:1–8. https://doi.org/10.1109/PESGM.2012.6345637.

[29] Nguyen L, Metzger M. Comparison of forecasting methods for vertical axis wind turbine applications in an urban/suburban area. J Renew Sustain Energy 2017;9. https://doi.org/10.1063/1.4978304.

[30] Zhou J, Shi J, Li G. Fine tuning support vector machines for short-term wind speed forecasting. Energy Convers Manag 2011;52:1990–8. https://doi.org/10.1016/j.enconman.2010.11.007.

[31] Luo X, Sun J, Wang L, Wang W, Zhao W, Wu J, et al. Short-term wind speed forecasting via stacked extreme learning machine with generalized correntropy. IEEE Trans Ind Informatics 2018;14:4963–71. https://doi.org/10.1109/TII.2018.2854549.

[32] Hong YY, Rioflorido CLPP. A hybrid deep learning-based neural network for 24-h ahead wind power forecasting. Appl Energy 2019;250:530–9. https://doi.org/10.1016/j.apenergy.2019.05.044.

[33] Data sheet collected from wind integrated substation – Kanjikode in Kerala, India.

[34] Technical Manual – Vestas V82 Wind Turbine,Vestas Wind Technology India Pvt. Ltd.

[35] Instruction Manual for MC31A - Three phase over current and Earth fault relay, Larsen and Turbo Limited, 2014.

[36] Upton E, Halfacree G. Raspberry Pi ® User Guide. John Wiley & Sons Ltd; 2012.